

The Quasar-frame Velocity Distribution of Narrow C IV Absorbers

D. Nestor,^{1,2,*} F. Hamann,² and P. Rodriguez Hidalgo²

* *dbn@ast.cam.ac.uk*

¹ *Institute of Astronomy, Madingley Road, Cambridge CB3 0HA, UK*

² *Department of Astronomy, University of Florida, Gainesville, FL, 32611, USA*

Accepted Received

ABSTRACT

We report on a survey for narrow (FWHM $< 600 \text{ km s}^{-1}$) C IV absorption lines in a sample of bright quasars at redshifts $1.8 \leq z < 2.25$ in the Sloan Digital Sky Survey. Our main goal is to understand the relationship of narrow C IV absorbers to quasar outflows and, more generally, to quasar environments. We determine velocity zero-points using the broad Mg II emission line, and then measure the absorbers’ quasar-frame velocity distribution. We examine the distribution of lines arising in quasar outflows by subtracting model fits to the contributions from cosmologically intervening absorbers and absorption due to the quasar host galaxy or cluster environment. We find a substantial number ($\geq 43 \pm 6$ per cent) of absorbers with $W_0^{\lambda 1548} > 0.3 \text{ \AA}$ in the velocity range $+750 \text{ km s}^{-1} \lesssim v \lesssim +12000 \text{ km s}^{-1}$ are intrinsic to the AGN outflow. This ‘outflow fraction’ peaks near $v = +2000 \text{ km s}^{-1}$ with a value of $f_{outflow} \simeq 0.81 \pm 0.13$. At velocities below $v \approx +2000 \text{ km s}^{-1}$ the incidence of outflowing systems drops, possibly due to geometric effects or to the over-ionization of gas that is nearer the accretion disk. Furthermore, we find that outflow-absorbers are on average broader and stronger than cosmologically-intervening systems. Finally, we find that ~ 14 per cent of the quasars in our sample exhibit narrow, outflowing C IV absorption with $W_0^{\lambda 1548} > 0.3 \text{ \AA}$, slightly larger than that for broad absorption line systems.

Key words: quasars: absorption lines – galaxies: active – intergalactic medium – accretion, accretion discs

1 INTRODUCTION

High speed outflows observed in rest-frame UV absorption lines are common components of active galactic nuclei (AGN). The ejected gas is believed to be driven off of the accretion disk around a central super-massive black hole (SMBH) by either radiation pressure (Proga et al. 2000 and 2004) or magneto-centrifugal ‘forces’ (Everett 2005). In luminous quasars, the outflows might be sufficiently energetic to provide important feedback to the galactic surroundings, potentially disrupting star formation and halting further growth of the SMBH (Hamann & Ferland, in prep., Hamann et al. 2007, Di Matteo et al. 2005, and refs. therein). Quasar outflows might also contribute to the blowout of gas and dust from young galaxies, and thereby help to distribute metals to the surroundings and reveal the central accreting SMBH as an optically visible quasar (Silk & Rees 1998, Moll et al. 2007).

Nonetheless, AGN outflows remain poorly understood. Most quasar studies have focused on the blueshifted broad

absorption lines (BALs), which very clearly identify powerful outflows at typical velocities of 5000 to 20000 km s^{-1} (Korista et al. 1993, Weymann et al. 1991). BALs are detected in ~ 10 per cent of optically-selected quasars (Trump et al. 2006), but the flows themselves might be ubiquitous if, as expected, the absorbing gas subtends just a fraction of the sky as seen from the central continuum source (e.g., Hamann et al. 1993).

There is, however, a wider range of observed outflow phenomena than just the BALs. For example, there are the so-called ‘associated’ absorption lines (AALs) that appear in roughly 25 per cent of quasar spectra (see also Vestergaard 2003). These features are much narrower than the BALs, with full widths at half minimum (FWHMs) of several hundred km s^{-1} or less, and they have redshifts that are, by definition, within a few thousand km s^{-1} of the emission line redshift, i.e., $z_{abs} \approx z_{quasar}$ (e.g., Foltz et al. 1986, Anderson et al. 1987). However, unlike the BALs, the identification of AALs with quasar outflows is often ambiguous. Weymann et al. (1979) noted that AALs can have a variety of origins,

including quasar host galaxies or cluster environments, and cosmologically intervening (unrelated) material, in addition to quasar outflows. Nonetheless, there is growing evidence that a substantial fraction of AALs and other narrow absorption lines (NALs) at even larger velocity shifts do form in quasar outflows. In their sample of 66 quasar spectra, Weymann et al. measured a strong excess of C IV systems with $z_{abs} \simeq z_{quasar}$ compared to $z_{abs} \ll z_{quasar}$. Although the statistics were somewhat poor, they measured a quasar rest-frame velocity width for this excess of $\approx 1200 \text{ km s}^{-1}$, centred near $v = 0$, which they attributed to the quasar cluster environment, and a significant tail extending out to blueshifts of $\approx 15000 \text{ km s}^{-1}$ which they identified with an ejected/outflow component.

More recently, Richards (2001) found a ~ 36 per cent excess of narrow C IV absorbers with $v > 5000 \text{ km s}^{-1}$ in flat-spectrum quasars as compared to steep-spectrum quasars. This was interpreted as evidence that over a third of high-velocity NALs are ejected from quasars. Well-studied individual cases provide direct evidence for an outflow origin of some NALs based on, for example, variable line strengths, resolved line profiles that are smooth and very broad compared to the thermal speeds, and doublet strength ratios showing that the absorber covers only part of the background light source along our observed sightlines (e.g., Hamann et al. 1997a and 1997b, Barlow & Sargent 1997, Misawa et al. 2007, and refs. therein). Two variability studies, in particular, indicate that at least ~ 21 per cent of quasar AALs form in the inner, dynamic regions of quasar outflows (Narayanan et al. 2004, Wise et al. 2004).

Determinations of the detection frequency and the velocity distribution of ejected NALs are essential to our understanding of the basic structure and physics of quasar outflows. These results will also impact studies of intervening systems. Cosmologically intervening C IV absorbers are used to study galaxy halos and the enrichment history of the IGM (e.g., Songaila, 2001; Ryan-Weber, Pettini & Madau, 2006; etc.) Determining the contamination of intervening samples by intrinsic absorbers is therefore pertinent to those studies.

With the goal of mapping the incidence of narrow C IV absorption in quasar rest-frame velocity space, we make use of the large publicly available spectroscopic database from the Sloan Digital Sky Survey (SDSS; York et al., 2000). In §2 we describe our data set. In §3 we describe the analyses of the absorber catalog and possible systematic effects, in §4 we discuss the implications of our results and in §5 we summarize our conclusions.

2 DATA SET

2.1 The Quasar Sample

We selected quasar spectra from the 4th data release of the SDSS. The spectra cover a wavelength range of 3820\AA (with resolution $R = 1800$) to 9200\AA ($R = 2100$), corresponding to C IV redshifts of $z_{abs} > 1.468$ and resolutions of $143 \text{ km s}^{-1} \leq \delta v \leq 167 \text{ km s}^{-1}$. We wish to study absorbers over a large span of quasar-frame velocities, from negative velocities (i.e., redshifted with respect to the quasar) to large ($\approx 71000 \text{ km s}^{-1}$) positive velocity corresponding to the red-edge of

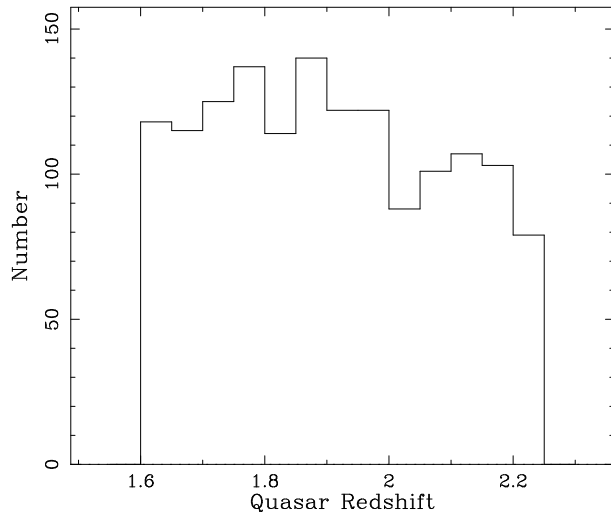


Figure 1. The redshift distribution of our quasar sample.

the Ly α emission.¹ To cover this complete range requires $z_{quasar} > 2.14$. However, in order to accurately measure the quasar redshifts (see §2.2 below), we require $z_{quasar} < 2.25$ so that the quasar Mg II emission line is covered by the data. Furthermore, the number of high signal to noise ratio (S/N) spectra available decreases with increasing redshift. Therefore, to maximize the sample size while balancing velocity coverage against S/N, we adopt a minimum quasar redshift of $z_{quasar} = 1.8$. We select the 1000 quasars with the highest median S/N in the r' -band that meet the above redshift criteria, as returned by the DR4 spectroscopic query form. This selection results in a sample with r' -band S/N ≥ 17.9 in each spectrum.

The incidence of absorbers at relatively low quasar-frame velocity is of particular interest. Therefore, in order to increase the sample size at low-velocity, we select an additional 500 spectra with $1.6 \leq z_{quasar} \leq 1.8$. These had r' -band S/N ≥ 18.7 in each spectrum. The emission redshift distribution of the total sample of 1500 quasars is shown in Fig. 1.

2.2 Velocity zero-point determination

As quasar broad emission lines are typically blueshifted from the systemic (centre-of-mass) redshift of the AGN, with the amount of the shift varying from line to line (e.g., Tytler & Fan 1992; Vanden Berk et al. 2001), it is a non-trivial matter to determine accurate velocity zero-points in individual spectra. The SDSS determines quasar redshifts using an automated algorithm (Stoughton et al., 2002) to perform a weighted matching of detected emission lines to empirically-determined wavelengths from the composite spectrum of Vanden Berk et al. These empirical wavelengths, which generally differ from laboratory wavelengths, are determined assuming that [O III] represents the systemic redshift. According to Schneider et al. (2002), the statistical error (measured

¹ Absorber-quasar velocity differences greater than $\approx 71100 \text{ km s}^{-1}$ place the C IV $\lambda 1548$ absorption feature in the Ly α forest, making identification and measurement prohibitively difficult.

from the scatter from the individual lines or the height and width of the cross-correlation function) in this method is less than $\delta_z \simeq 0.01$ ($\delta_v \simeq 1000 \text{ km s}^{-1}$) RMS for non-BAL quasars and $\delta_z \simeq 0.01\text{--}0.03$ ($\delta_v \simeq 3000 \text{ km s}^{-1}$) for BAL quasars. Additionally, there are also very likely to be systematic errors that depend on which lines are covered, and thus depend on redshift in a non-straightforward manner. Thus, because accurate velocity zero-points are important to this study, the SDSS-provided redshifts are insufficient for our purposes.

It has been shown, however, that the Mg II broad emission line has both a relatively small average offset from [O III] ($\langle \Delta v_{\text{Mg II}} \rangle \sim 0 \pm 100 \text{ km s}^{-1}$) and a relatively small quasar-to-quasar scatter in the offset ($\sigma_{\Delta v} \lesssim$ a few hundred km s^{-1}) compared to other broad emission lines. The use of Mg II-derived redshifts should therefore reduce the dispersion between the measured and true values of the quasar-frame absorption velocities and thus increase the precision of our measurements. Even more important than reducing the scatter in the measured velocities, however, is to remove any systematic shift by using an accurate and appropriate average velocity-offset of the Mg II emission line relative to [O III]. Tytler & Fan give a value for this offset of $\langle \Delta v_{\text{Mg II}} \rangle = +101 \text{ km s}^{-1}$ with a dispersion of $\sigma_{\Delta v} = 92 \text{ km s}^{-1}$, where positive velocity indicates a blueshift with respect to [O III]. Richards et al. (2002), however, find $\langle \Delta v_{\text{Mg II}} \rangle = -97 \text{ km s}^{-1}$ and $\sigma_{\Delta v} = 269 \text{ km s}^{-1}$. The Richards et al. results are derived from a large sample and, like the present study, using SDSS data, but with quasars at significantly lower redshift than used here. McIntosh et al. (1999) and Scott et al. (2000) provide data at higher redshift using near-infrared spectra; we made use of the nineteen high- z values from these two sources and find $\langle \Delta v_{\text{Mg II}} \rangle = +102 \text{ km s}^{-1}$, but with a large dispersion. Removing one outlier reduces the dispersion and gives $\langle \Delta v_{\text{Mg II}} \rangle = -1 \text{ km s}^{-1}$.

Clearly there is no consensus value for either the offset or the quasar-to-quasar dispersion in the offset. Thus, we conduct all of our analyses using four different techniques for determining quasar redshifts (and thus velocity zero-points): Mg II-determined redshifts using Mg II zero-point offsets of 0 km s^{-1} (i.e., no Mg II velocity-offset from [O III]), $+102 \text{ km s}^{-1}$ and -97 km s^{-1} , as well as the SDSS redshift values. We adopt the value $\sigma_{\Delta v} = 269 \text{ km s}^{-1}$ from Richards et al. as our zero-point uncertainty, which represents the true scatter in the Mg II-[O III] velocity offset convolved with the uncertainty in the ability to fit the Mg II emission in the SDSS data. Our interactive fitting (described below) is likely superior to the automated routine employed by the SDSS pipeline. However, comparison of our values to those from the SDSS database indicate the improvement is in most cases small, and thus the adopted value of $\sigma_{\Delta v} = 269 \text{ km s}^{-1}$ is likely a fair estimate of our zero-point uncertainty.

To compute the Mg II-determined redshifts, we fitted a Gaussian to the Mg II emission line for each quasar in our sample, assuming the given velocity zero-point offset. The fits made use of only the central peak of the emission line in order to avoid effects from line-asymmetries. In practice, the extent of the fitted region varied, depending on the emission line profile. The precision with which we were able to determine the peak wavelength also depended on the profile. The formal (i.e., fitting) errors were typically $< 10 \text{ km s}^{-1}$. While the actual Mg II zero-point uncertainties

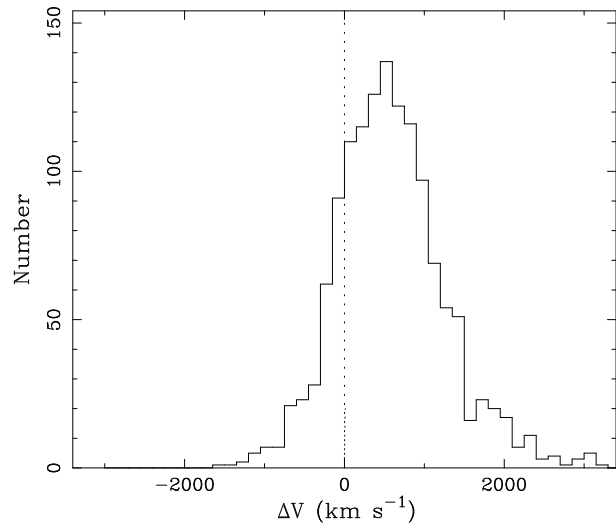


Figure 2. The velocity zero-point correction distribution of our quasar sample for $\langle \Delta v_{\text{Mg II}} \rangle = 0 \text{ km s}^{-1}$. Positive velocities correspond to our Mg II-corrected redshift being larger than the SDSS redshift. The distribution has a mean of $+582 \text{ km s}^{-1}$ and a standard deviation of 684 km s^{-1} .

are necessarily larger than this, they are in most cases always well below the dispersion as described above. Such fits were possible in 92 per cent of the sample; while the Mg II emission in the remaining 8 per cent was too weak and/or noisy (e.g., due to poorly subtracted night-sky lines) to determine an accurate fit. For these systems, we applied an assumed zero-point correction equal to the average correction of the Mg II-fitted sample. The distribution of velocity zero-point differences (compared to the SDSS values) for the re-determined redshifts is shown in Fig. 2 for no Mg II velocity zero-point offset. Positive velocities correspond to our Mg II-derived redshift being larger than the SDSS redshift. The distribution has a median value of $+545 \text{ km s}^{-1}$, a mean of $+582 \text{ km s}^{-1}$ and a standard deviation of 684 km s^{-1} . The velocity zero-point difference distribution for the SDSS-provided redshifts and those determined from the Mg II emission fits in the SDSS database is almost identical to Fig. 2, except for a large spike at $+1500 \text{ km s}^{-1}$ as the SDSS line-fitting algorithm does not allow shifts larger than this value.

2.3 Identification and measurement of C IV absorbers

We fit pseudo-continua (including the broad emission lines) to each spectrum and identify C IV absorber candidates using software described in Nestor, Turnshek & Rao (2005), updated and adjusted to apply to C IV. Each continuum-fit was visually inspected and, when necessary, interactively re-fit. Approximately 2 per cent of the quasars in our sample were either misclassified stars or exhibited BAL absorption strong enough that there was little unabsorbed flux in the spectral regions of interest and accurate continuum-fitting proved impossible. These objects were removed from the sample.

The software used to identify C IV candidates is very sensitive to narrow absorption; therefore we are confident

that all narrow absorbers above our significance level threshold ($\geq 5\sigma$ for the $\lambda 1548$ line and $\geq 3\sigma$ for $\lambda 1551$, see Nestor et al. 2005) were found. Each candidate was visually inspected to remove redundant and false detections. Care was taken to avoid misclassifying the low-ionization pair C I $\lambda 1277$ and O I $\lambda 1302$, which has a similar separation to the C IV doublet, as high-velocity ($v \gtrsim 48000 \text{ km s}^{-1}$) C IV absorption. Furthermore, the Ly α and N V blended emission lines occasionally led to difficulties for our continuum-fitting software. Thus, while we did not exclude these regions when detecting and measuring absorbers, we conservatively restrict the analyses in this paper to velocities $v \leq 60000 \text{ km s}^{-1}$ in order to avoid potential biases.

The large majority of the C IV absorbers that we identified in our sample were straightforward to measure. However, there are also many systems exhibiting broad, resolved profiles. Furthermore, as C IV absorption is relatively common in quasar spectra, blending of systems at similar redshifts is occasionally a problem in the medium resolution SDSS spectra, particularly at low-velocity ($z_{abs} \approx z_{quasar}$) where there is an excess of absorbers (see below). While highly accurate rest equivalent width (W_0) and FWHM measurements are not crucial for the purposes of this paper, proper *counting* of systems is very important. It is typical in studies of intervening absorbers to designate a minimum velocity separation for which two absorbers are counted separately. However, series of systems at low-velocity can be blended across large velocity ranges, and narrow systems can be partially blended with broad systems, making the effective separation for which it is possible to discern separate systems widely variable. Therefore, we took the following approach, that will be described in greater detail in Rodriguez Hidalgo, Hamann & Nestor (in prep.) To each system we fit a Gaussian pair having the correct C IV doublet separation, the same FWHM, and a $\lambda 1548 : \lambda 1551$ doublet ratio constrained to the range 1 : 1 to 2 : 1. When absorbers appeared to have distinct but blended components, we simultaneously fit multiple pairs to the entire blended profile, with each component fit with a single Gaussian doublet pair and considered as a distinct absorption system. In order to decide the number of components to fit, we always used the minimum number justifiable by the data; that is, we only added an additional component when there was clear evidence for a separate absorption feature (member of a doublet). In some cases, broad components were not well described by a single Gaussian pair, but the data did not justify deblending into multiple features according to our counting rules. Nonetheless, a single Gaussian pair per component always provided a reasonable estimate of both W_0 and FWHM for the system in question. Since the problematic systems are exclusively broad, they do not enter into the analysis described in this paper.

3 ANALYSIS

3.1 Defining the narrow C IV sample

For the present study, we want to exclude the more obvious outflows lines, the BALs and mini-BALs (§1). We therefore removed from our sample all absorbers with measured FWHM $> 600 \text{ km s}^{-1}$. We also removed all absorbers

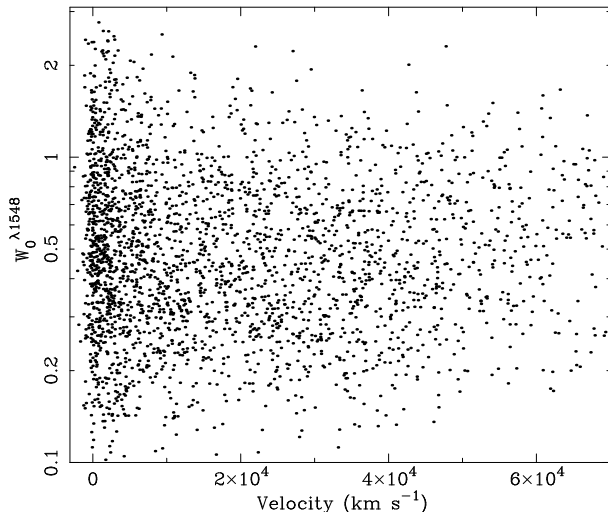


Figure 3. Scatter-plot of $W_0^{\lambda 1548}$ versus quasar-frame velocity for our narrow ($\text{FWHM} \leq 600 \text{ km s}^{-1}$) absorber sample. Velocities shown are for the Mg II-corrected redshifts assuming no Mg II velocity zero-point offset.

blended with absorbers having $\text{FWHM} > 600 \text{ km s}^{-1}$ as their identification can often be ambiguous. This helps reduce uncertainties associated with deblending and counting but, in the end, has little impact on our results because the number of such systems is small (< 1 per cent of the sample). Finally, several spectra in the sample contain extremely strong BAL absorption which removes flux from a large swathe of continuum. We computed both the BALnicity Index (BI; Weymann et al. 1991) and the Absorption Index (AI; Hall et al. 2002) to quantify these absorbers (see Rodriguez Hidalgo et al. for more discussion). After visual inspection, it was decided to remove spectra with $\text{AI} > 3120$ and/or $\text{BI} > 1250$, which totaled 62 quasars. We note that this is *not* the equivalent of removing BAL quasars; rather, we remove only those with little ‘usable’ unabsorbed continuum (although, for the BAL quasars kept in the sample, we do not include narrow C IV systems that are blended with BALs.)

The final sample includes 1409 quasars, which provide a catalog of 2566 narrow C IV absorbers with $0.1 < W_0^{\lambda 1548} < 2.8 \text{ \AA}$ and $-3000 < v_{abs} < 70000 \text{ km s}^{-1}$, 2009 of which have $W_0^{\lambda 1548} > 0.3 \text{ \AA}$. We note that $W_0^{\lambda 1548}$ and FWHM are correlated, so the removal of $\text{FWHM} > 600 \text{ km s}^{-1}$ systems biases our catalog against very strong systems. Figure 3 shows a scatter-plot of $W_0^{\lambda 1548}$ versus quasar-frame velocity for the final narrow C IV catalog.

3.2 Computing the completeness correction

Our data set is complete in neither $W_0^{\lambda 1548}$ or velocity-space. It is therefore necessary to compute a two-dimensional completeness correction. We follow a procedure similar to that described in Nestor et al. (2005), whereby we determine the minimum $W_0^{\lambda 1548}$, W_{min} , detectable at our imposed significance-level threshold at every pixel and half-pixel in each spectrum. We then construct an array on a grid of velocity and $W_0^{\lambda 1548}$ steps with values corresponding to the number of spectra for which a C IV $\lambda 1548$ line of the given

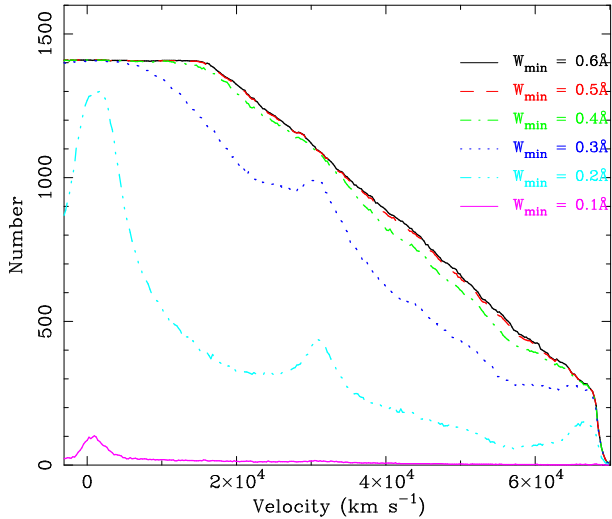


Figure 4. The number of usable spectra as a function of velocity corresponding to $W_0^{\lambda 1548}$ values of 0.1 Å, 0.2 Å, 0.3 Å, 0.4 Å, 0.5 Å and 0.6 Å, using Mg II-corrected redshifts assuming no Mg II velocity-offset. The 0.5 Å and 0.6 Å curves are nearly identical – above $W_0^{\lambda 1548} \simeq 0.5$ Å our sample is complete in $W_0^{\lambda 1548}$ at all velocities.

$W_0^{\lambda 1548}$ could have been detected at the given velocity, accounting for the removed regions of spectra having absorbers with $\text{FWHM} > 600 \text{ km s}^{-1}$. This ‘completeness array’ can then be used to correct any computed incidence of absorbers in both $W_0^{\lambda 1548}$ and velocity space. In Fig. 4 we show the number of usable spectra as a function of velocity for different minimum $W_0^{\lambda 1548}$ values. The 0.5 Å and 0.6 Å curves are nearly identical – above $W_0^{\lambda 1548} \simeq 0.5$ Å our sample is complete in $W_0^{\lambda 1548}$ at all velocities. Although the minimum detectable $W_0^{\lambda 1548}$ depends, in principle, on the absorption FWHM, in practice it is computed assuming unresolved lines. However, any detection bias arising from this would only be relevant for lines with $W_0^{\lambda 1548} \simeq W_{\min}$ that are also resolved in velocity. However, lines weaker than $\simeq 0.5$ Å (the strength above which our survey is complete) are generally unresolved in the SDSS spectra.

3.3 Results

3.3.1 The quasar-frame velocity distribution

Using the completeness array together with the absorber catalog, we can compute the incidence of absorbers as a function of velocity, $\frac{\partial n}{\partial \beta}$, where $\beta = v/c$. The magnitude of $\frac{\partial n}{\partial \beta}$ represents the average number of absorbers per km s^{-1} times the speed of light. Thus the average number of absorbers per spectrum can be found by integrating $\frac{\partial n}{\partial \beta}$ over the relevant velocity range:

$$\langle n \rangle = \frac{1}{c} \int_{V_{\min}}^{V_{\max}} \frac{\partial n}{\partial \beta} dv. \quad (1)$$

We show $\frac{\partial n}{\partial \beta}$ for $W_0^{\lambda 1548} \geq 0.3$ Å, using Mg II-corrected redshifts and assuming no Mg II velocity-offset, in Fig. 5. A large excess at $v \approx 0$ (i.e., $z_{\text{abs}} \simeq z_{\text{quasar}}$) is clearly detected. The observed distribution includes contributions from: (i) cosmologically-‘intervening’ systems; (ii) ‘environ-

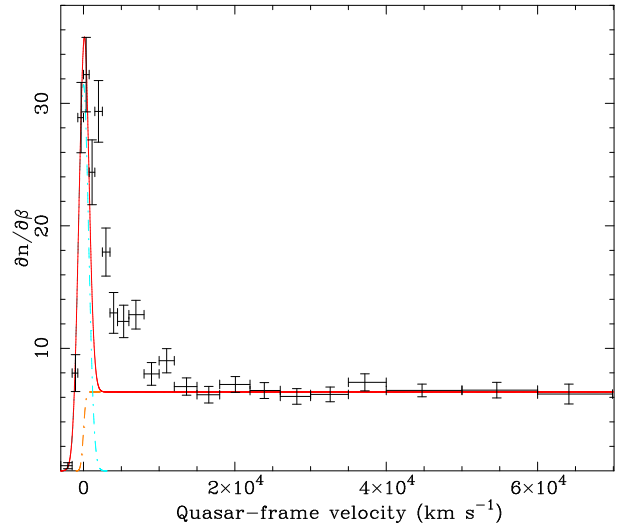


Figure 5. The incidence of CIV absorbers versus quasar-frame velocity for systems with $W_0^{\lambda 1548} \geq 0.3$ Å, using Mg II-corrected redshifts and assuming no Mg II velocity-offset. Horizontal bars indicate the velocity bins and vertical bars the 1σ uncertainty from counting statistics. The curves are maximum-likelihood fits to the data in the intervals $v < 0$ and $40000 \text{ km s}^{-1} < v < 60000 \text{ km s}^{-1}$, representing the ‘environmental’ and ‘intervening’ components, respectively (see text).

mental’ absorption which arises in either the ISM of the AGN host galaxy or the IGM of the galaxy’s group/cluster; and (iii) ‘outflow’ systems that are ejected from the central AGN (e.g., accretion-disk outflows). We model the intervening contribution to the distribution with a step function that breaks at $v = 0$, convolved with the redshift uncertainty (modeled as a Gaussian with $\sigma_z = 269 \text{ km s}^{-1}$). We model the environmental contribution with a Gaussian centred at $v = 0$. To obtain the best-fit parameters, we employ a maximum likelihood fit to the unbinned data (absorber catalog plus completeness array), using only data with $v < 0$ and $40000 \text{ km s}^{-1} < v < 60000 \text{ km s}^{-1}$ to constrain the fit, where the outflow fraction is *assumed* to be insignificant at these velocities. The physical velocity dispersion of the AGN-host’s local environment can be estimated from the environmental-component by deconvolving the Gaussian fit with the assumed redshift uncertainty (269 km s^{-1}) and, following Weymann et al., divide by $\sqrt{2}$ to account for the fact that what we measure is the difference between the velocity of the AGN-host within the environment and that of the other halos (although the appropriateness of this last step is limited by the presence of absorption in the AGN host galaxy, which is not virialized in the local environment).

The parameters describing the fits are shown in Table 1 for each zero-point determination method (§2.2). The first column indicates the velocity zero-point offset (for the Mg II-determined redshifts cases), and the parameters are defined by:

$$\frac{\partial n_{\text{env}}}{\partial \beta} = N_{\text{env}} \times \exp(-v^2/2\sigma_{\text{env}}^2), \quad (2)$$

$$\sqrt{2} \times \sigma'_{\text{env}} = \sqrt{\sigma_{\text{env}}^2 - (269 \text{ km s}^{-1})^2}, \quad (3)$$

and

Table 1. Environmental and intervening fit-parameters.

$\langle \Delta v_{\text{Mg II}} \rangle$ (km s^{-1})	N_{env}	σ_{env} (km s^{-1})	σ'_{env} (km s^{-1})	N_{inter}
0	31.5	681	442	6.4
+102	26.8	665	430	6.4
-97	35.4	694	452	6.4
SDSS	25.9	1319	913	6.5

The σ_{env} values are the Gaussian widths before and after deconvolution and the N values are the normalization of the fits – i.e., the incidence for intervening systems and the incidence of environmental systems at $v = 0$.

$$\frac{\partial n_{\text{inter}}}{\partial \beta} = N_{\text{int}}. \quad (4)$$

Our assumption that *none* of the absorbers at $v > 40000 \text{ km s}^{-1}$ or $v < 0$ arise in outflows means that our derived outflow fractions (see below) are strictly speaking lower limits at all velocities. For example, Richards et al. claim that as many as 36 per cent of C IV absorbers at $5000 < v < 55000 \text{ km s}^{-1}$ form in outflows, while Misawa et al. (2007) claim that the fraction of outflow lines at these velocities is $\simeq 10$ –17 per cent. However, it is unclear what the contribution of very high- v systems (i.e., $v > 40000 \text{ km s}^{-1}$) to the Richards result is, and the Misawa et al. sample contains no systems at $v > 40000 \text{ km s}^{-1}$ that are classified as a reliable narrow-line outflow candidates. Thus, while we cannot directly test our high velocity assumption, it is likely that we are only slightly, if at all, overestimating the contribution of intervening systems.

The assumption that all $v < 0$ absorbers are environmental is potentially less reliable, however. It will be an appropriate assumption if there are no ‘in-falling’ systems intrinsic to the AGN flow and all of the individual quasar velocity zero-points are accurate (or that there are no outflowing systems with velocities that are small relative to the velocity zero-point dispersion). However, our zero-points are inaccurate with an (assumed) RMS of $\sim 270 \text{ km s}^{-1}$, and the systematic velocity-offset of Mg II from the true velocity zero-point is not well constrained (see §2.2). Thus it is possible that our environmental fits are also accounting for some low-velocity outflow systems. We investigate this issue below.

The uncertainty in the appropriate velocity zero-point has a direct effect on the measured velocity-space distribution of absorbers. In order to determine the magnitude of this potential bias and investigate its affect on the computed outflow fraction, we computed $\frac{\partial n}{\partial \beta}$ as well as the maximum-likelihood fits using all four of the quasar redshift determination methods discussed in §2.2. Fig. 6 shows the low-velocity region of $\frac{\partial n}{\partial \beta}$ computed using: Mg II-determined redshifts with (a) no Mg II velocity zero-point offset (i.e., $\langle \Delta v_{\text{Mg II}} \rangle = 0$), (b) $\langle \Delta v_{\text{Mg II}} \rangle = +102 \text{ km s}^{-1}$, (c) $\langle \Delta v_{\text{Mg II}} \rangle = -97 \text{ km s}^{-1}$, as well as (d) SDSS redshifts. The curves represent the data well in the fit-regions, for all of the offsets considered. However, the distribution determined assuming $\langle \Delta v_{\text{Mg II}} \rangle = -97 \text{ km s}^{-1}$ overpredicts the incidence at $v \gtrsim 0$. We note that, if the velocity zero-point is (on average) properly determined, the incidence for $v \gtrsim 0$ should be larger than that for $v \lesssim 0$, since the $v \gtrsim 0$ data contains, in prin-

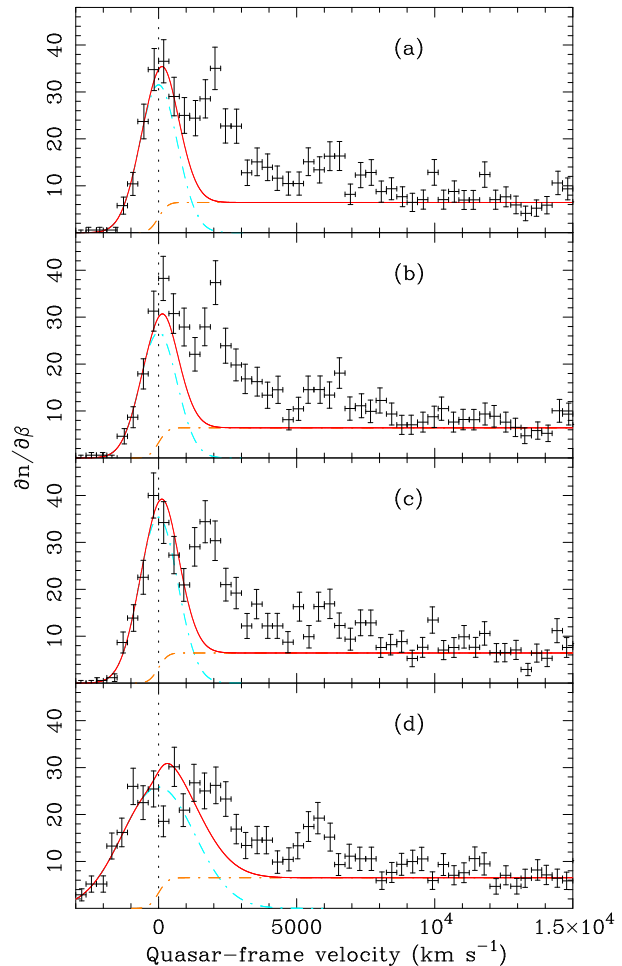


Figure 6. Same as Fig. 5, employing Mg II-determined redshifts with (a) no Mg II velocity zero-point offset, (b) $\langle \Delta v_{\text{Mg II}} \rangle = +102 \text{ km s}^{-1}$, (c) $\langle \Delta v_{\text{Mg II}} \rangle = -97 \text{ km s}^{-1}$, as well as (d) the SDSS-provided redshifts. The width of the environmental-component determined from SDSS redshifts is unphysically large, and that determined assuming $\langle \Delta v_{\text{Mg II}} \rangle = -97 \text{ km s}^{-1}$ gives a poor fit to the $v \sim 0$ data.

ciple, environmental, intervening, and outflowing C IV systems, and we assume the environmental-component is reasonably symmetric about the true velocity zero-point. We obtain a value of $\sigma'_{\text{env}} = 913 \text{ km s}^{-1}$ using the SDSS redshifts, which is unphysically large unless the quasar environments are predominantly in large clusters (e.g., Becker et al. 2007). However, Outram et al. (2003) show that the clustering amplitude of quasars at $z \sim 1.4$ is similar to that of present-day galaxies. The Mg II-determined redshifts lead to values of $430 \lesssim \sigma'_{\text{env}} \lesssim 450 \text{ km s}^{-1}$ for the dispersion, which is comparable to the usual division between large groups and poor clusters (e.g., Mulchaey, 2000).

Considering the quality of the fits, we conclude that, while we do not explicitly reject any of the Mg II-corrected redshift choices, an average Mg II velocity zero-point offset of $\simeq 0$ to $+100 \text{ km s}^{-1}$ is most appropriate for our sample. Except when explicitly stated, we will use $\langle \Delta v_{\text{Mg II}} \rangle = 0$ for the subsequent analyses. We also note that we computed $\frac{\partial n}{\partial \beta}$ for ranges of $W_0^{\lambda 1548}$, but found no significant trends.

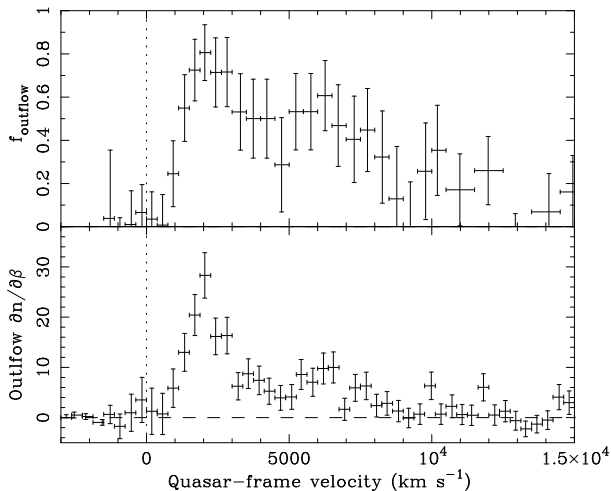


Figure 7. Top: The excess of the data over the sum of the two fits, divided by the data, which represents the minimum outflow fraction. Bottom: The data minus our fits to the environmental and intervening systems, representing $\frac{\partial n}{\partial \beta}$ for the ejected (i.e., outflow) component only.

3.3.2 The outflow fraction and incidence of outflowing absorbers

The top panel of Fig. 7 shows the data minus the sum of the two fits, divided by the data, which represents the minimum outflow fraction, $f_{outflow}$ (which is considered a minimum for the reasons described above). We find that $f_{outflow}$ increases strongly from $v = 0$ to $v \simeq +2000 \text{ km s}^{-1}$, where it peaks with $f_{outflow} \simeq 0.81 \pm 0.13$, and then decreases slowly out to $v \sim +12000 \text{ km s}^{-1}$. Over the range where there is significant evidence for a non-zero outflow fraction, $v \simeq +750 \text{ km s}^{-1}$ to $v \approx +12000 \text{ km s}^{-1}$, we find $\langle f_{outflow} \rangle = 0.43 \pm 0.06$. Over narrower ranges near the peak, we find $\langle f_{outflow} \rangle = 0.57 \pm 0.10$ for $+1250 \text{ km s}^{-1} < v < +6750 \text{ km s}^{-1}$, and $f_{outflow} \simeq 0.72 \pm 0.07$ for $v \simeq +1250 \text{ km s}^{-1}$ to $v \approx +3000 \text{ km s}^{-1}$. The outflow fraction decreases below $v \approx +2000$ and disappears below $v \approx +750$, apparently indicating an effective minimum projected ejection velocity for narrow C IV systems. It is also possible that systematics such as a strong proximity effect for the intervening absorbers or limitations in our ability to properly count systems contribute to this decrease. We discuss these and other possible biases in §3.4.

In the bottom panel of Fig. 7 we show the data after subtraction of the sum of the fits (using $\langle \Delta v_{\text{Mg II}} \rangle = 0$), which represents $\frac{\partial n}{\partial \beta}$ for the outflow-component only. Using $\langle \Delta v_{\text{Mg II}} \rangle = -97 \text{ km s}^{-1}$ (i.e., Mg II emission redshifted from the quasar rest-frame) or SDSS-determined redshifts leaves, respectively, marginally- and strongly-statistically significant negative, and thus unphysical, residual incidence for the outflow-component at some velocities. Using $\langle \Delta v_{\text{Mg II}} \rangle = 0$ (i.e., Mg II emission unshifted from the quasar rest-frame), the incidence of systems is consistent with zero at low positive velocities: in this case, our assumptions that no absorbers arising in outflows have measured velocities with $v < 0$ is likely valid. Attempts to fit the entire span of velocities (i.e., including $0 < v < 40000 \text{ km s}^{-1}$, see §3.3.1) with, e.g., a power-law or exponential for $v > 0$, failed since,

as is clear from the bottom panel of Fig. 7, these were not appropriate descriptions of the outflowing component. Considering the results employing Mg II-corrected quasar redshifts, we find that the incidence of narrow C IV absorbers with $W_0^{\lambda 1548} > 0.3 \text{ \AA}$ presumably forming in accretion-disk outflows peaks at $v \simeq 2000 \text{ km s}^{-1}$ and exhibits a wing that extends out to at least $v \simeq 9000 \text{ km s}^{-1}$, for all $\langle \Delta v_{\text{Mg II}} \rangle$ values considered.

3.4 Possible systematics

In this section we discuss potential biases introduced by the method we employ to ‘count’ systems as well as the assumptions behind the modeling of the distribution of cosmologically-intervening absorbers.

As narrow C IV absorbers cluster at low ($\lesssim 1000 \text{ km s}^{-1}$) quasar-frame velocities (Nestor, Hamann & Rodriguez Hidalgo, 2007), removing regions with broad absorption is more likely to also remove narrow absorbers, compared to randomly selected regions at similar velocity. Since broad absorbers are more common at low positive velocity, it is a concern that this bias may affect the measured distribution of narrow systems. Furthermore, this region of velocity space exhibits (in principle) all three of our categories of absorbers, thus increasing the chances for blending of outflow and non-outflow systems to occur. Therefore, the apparent dearth of narrow outflow-component systems at $v \lesssim 2000 \text{ km s}^{-1}$ (Fig. 7) could conceivably be in part a byproduct of our removal of broad systems and absorbers blended with broad systems. To test this, we re-computed $\frac{\partial n}{\partial \beta}$ without rejecting *any* absorbers based on FWHM or blending with broad systems. However, the only qualitative difference in our results was an extension of the high-velocity tail of outflowing systems out to $v \approx 25000 \text{ km s}^{-1}$, indicating that broad (FWHM $> 600 \text{ km s}^{-1}$) absorbers have a larger extent in ejection-velocity than do narrow systems. This will be discussed in further detail in Rodriguez Hidalgo, Hamann & Nestor (in prep.)

Alternatively, over-zealous de-blending could, conceivably, influence both the shape and magnitude of $\frac{\partial n}{\partial \beta}$. To investigate this concern, we combined all absorbers with velocity differences less than the sum of the two HWHM values plus 150 km s^{-1} (i.e., the SDSS resolution) into a single absorber to be counted once. We then recomputed $\frac{\partial n}{\partial \beta}$ and the fits with this reduced catalog. This resulted in a slight decrease in the outflow fraction for bins where it was non-zero, and virtually no change in the shape or range over which $f_{outflow} > 0$ is significant. Even when we took the extreme step of combining all absorbers within 500 km s^{-1} plus the sum of the two HWHM values, the shape of $\frac{\partial n}{\partial \beta}$ for outflow-only systems remained the same, although the magnitude was reduced by $\simeq 20 - 25$ per cent. Thus, we believe that any inconsistencies in our counting method is at a level small enough to be safely ignored.

Another concern is that cosmologically-intervening systems may not be uniformly distributed in quasar-frame velocity for our quasar sample. For example, it is known that at high- z the incidence of intervening C IV absorbers decreases with increasing redshift (Sargent, Boksenberg & Steidel, 1988; Misawa et al., 2002). Larger redshift correlates with smaller velocity in Figs. 5-7. According to Monier et al. (2006), the incidence of $W_0^{\lambda 1548} \geq 0.3 \text{ \AA}$ systems show

little evolution over the range $1.46 < z < 2.25$. Misawa et al., however, claim a $\simeq 50$ per cent decrease over the same range. While the decrease in $f_{outflow}$ is too abrupt to be entirely caused by redshift effects, we nonetheless investigated the maximum possible magnitude of this effect by running 50 Monte Carlo simulations of intervening systems in our data. We randomly distributed absorbers in the spectra of our sample in redshift-space using the $\frac{\partial n}{\partial z}$ parameterization from Misawa et al., and converted the resulting distributions into velocity-space to determine the modelled $\frac{\partial n}{\partial \beta}$. This resulted in $\lesssim 10$ per cent decrease in $\frac{\partial n}{\partial \beta}$ from $v \approx 45000$ km s^{-1} to $v = 0$, or a difference of $\lesssim 0.7$ in $\frac{\partial n}{\partial \beta}$.

Potentially more important is the possibility of a strong proximity effect, similar to that seen for Lyman- α forest lines, causing a decrease in $\frac{\partial n}{\partial \beta}$ for the intervening systems. While the magnitude of any proximity effect likely depends on the line-strengths being considered, C IV has a much higher ionization energy than does H I (64.5 eV compared to 13.6 eV) and thus any C IV proximity effect should be significantly weaker than that for H I. Thus, we ran 50 additional Monte Carlo simulations of intervening systems using the proximity effect results for the Lyman- α forest from Scott et al. (2000), considering this a strong upper-limit to any C IV proximity effect. Doing so, we find a linear decrease in $\frac{\partial n}{\partial \beta}$ from no difference at $v = 2000$ km s^{-1} to a 50 per cent deficit of systems at $v = 0$. This corresponds to a difference in $\frac{\partial n}{\partial \beta}$ at $v = 0$ of $\simeq 3.5$. Thus, a C IV proximity effect as strong as what is claimed for Lyman- α would only marginally change the results described above, and then only at $v \sim 0$.

Finally, we also considered the effect of an underestimation of the velocity zero-point dispersion. A larger dispersion would cause more low-velocity intervening systems to scatter to $v < 0$. We repeated the modeling of the environmental and intervening components doubling the velocity zero-point dispersion and found no qualitative changes to our results.

We are limited in our ability to determine true individual velocity zero-points, to deblend ('count') absorbers into physically-distinct systems with complete accuracy, and to know the true distributions of the non-outflowing absorber populations. These systematics almost certainly affect our results to some degree. Nonetheless, the maximum estimates of the effects from all of the systematics that we considered are relatively small and have no significant impact on our qualitative results.

4 DISCUSSION

4.1 Properties of the outflowing absorbers

We find a significant detection of narrow C IV absorption over that which is expected from cosmologically-intervening and host galaxy-environment contributions, putatively occurring in accretion disk winds, in the quasar-frame velocity range $750 \text{ km s}^{-1} \lesssim v \lesssim 12000 \text{ km s}^{-1}$. Using eqn. 1 together with the $\frac{\partial n}{\partial \beta}$ values for the outflow-component (Fig. 7), we can compute the average number of outflowing absorbers per quasar. We find $\langle n_{outflow} \rangle = 0.25 \pm 0.02$ using $\langle \Delta v_{\text{Mg II}} \rangle = 0$. The value depends only slightly on the choice of $\langle \Delta v_{\text{Mg II}} \rangle$ and the limits of integration.

While it is likely that some $W_0^{\lambda 1548} \geq 0.3 \text{ \AA}$ low-velocity ($\lesssim 750 \text{ km s}^{-1}$) narrow C IV absorbers arise in outflows, the

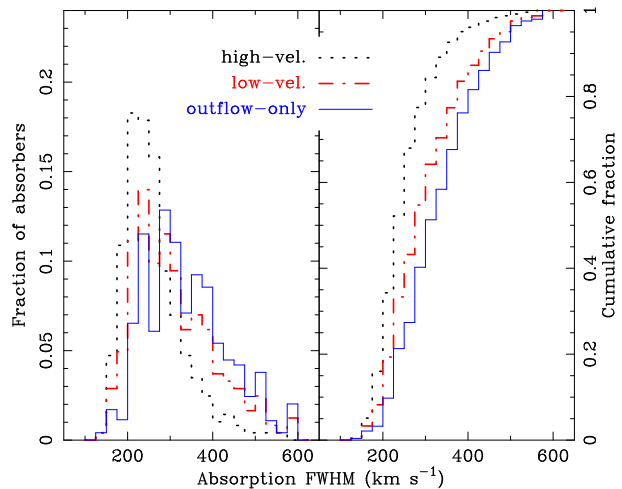


Figure 8. The normalized (left) and cumulative (right) FWHM distributions for high- and low-velocity absorber sub-samples. The low-velocity sample is clearly broader. Note that the SDSS resolution ($\simeq 150 \text{ km s}^{-1}$) sets the lower-limit seen in these data. Also shown (solid histograms) are the weighted difference distributions (using the measured outflow fraction, see text), which represents the distributions for outflowing-systems only.

various possible systematic effects discussed above are unable to completely, or even mostly, explain the turnover in $\frac{\partial n}{\partial \beta}$ for outflow-only absorbers below $v \lesssim 2000 \text{ km s}^{-1}$ – it appears rather to be an indication of a minimum projected line-of-sight ejection velocity for narrow C IV absorption systems in AGN outflows. This empirical phenomenon can help to constrain quasar outflow models. For example, the deficit of C IV outflow-systems at $v \lesssim 2000 \text{ km s}^{-1}$ might result from a tendency to ‘over-ionize’ the low-velocity gas, e.g., if that gas is typically nearer the ionizing continuum source than the high speed absorbers. This can occur in any model of the acceleration (radiation pressure or magnetocentrifugal forces), but over-ionization at low velocities has a direct physical explanation if there is radiative driving. In particular, highly ionized gas is more transparent and thus more difficult to push via radiation pressure. High flow-speeds are attained only in less ionized gas (that might be farther downstream in the flow and partially shielded from the intense ionizing radiation, e.g., Hamann & Ferland, in prep).

We can also infer the distribution of other outflow-absorber properties by comparing the high-velocity (intervening) absorbers to those at lower velocities where $f_{outflow} > 0$ but the incidence of environmental systems is negligible. To optimize such a comparison, we require a range of velocity large enough to include a significant number of outflowing absorbers, while restricting ourselves to velocities where the outflow fraction is high. Fig. 8 shows the normalized (left) and cumulative (right) distributions of FWHMs for absorbers with $1800 \text{ km s}^{-1} < v < 4400 \text{ km s}^{-1}$, over which the effective outflow fraction is $\langle f_{outflow} \rangle = 0.61 \pm 0.07$ and the environmental contribution is small, and $30000 \text{ km s}^{-1} < v < 60000 \text{ km s}^{-1}$, where we assume the absorbers to all be cosmologically intervening systems. The low-velocity FWHM distribution is clearly broader than the high-velocity distribution. A K-S test gives a zero per cent

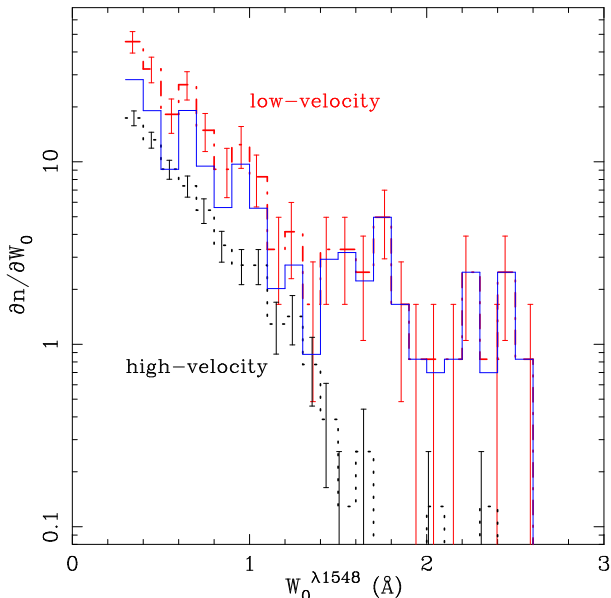


Figure 9. Incidence of absorbers as a function of $W_0^{\lambda 1548}$, for high- and low-velocity samples. Also shown (solid histogram) is the difference between the two distributions which represents the distribution for outflow-systems only.

probability that the two sets of data are drawn from the same parent distribution. A broader distribution is expected if the low-velocity sample contains outflowing absorbers. We also show in Fig. 8 the weighted (assuming $f_{outflow} = 0.61$), renormalized difference between the two distributions, which should represent the pure outflow distribution and has a mean $\langle \text{FWHM} \rangle = 337 \text{ km s}^{-1}$ – though we note that the SDSS resolution imposes an artificial lower-limit to the measured FWHM of $\approx 150 \text{ km s}^{-1}$. We also compared the distribution of $\lambda 1548 : \lambda 1551$ doublet-ratios (DR) for the two velocity sub-samples. The doublet ratio distributions are similar except that the low-velocity sample exhibits relatively more completely saturated absorbers: 26 ± 3 per cent with $DR > 0.9$ compared to 15 ± 2 per cent at high-velocity, which implies that a third (33 ± 6 per cent) of outflowing absorbers in this velocity range have $DR > 0.9$. This result implies that outflow systems contain fewer weak kinematically-distinct components that are unresolved in the SDSS spectra than do intervening absorbers. Although individual outflowing narrow C IV absorbers appear similar to non-intrinsic systems in low/medium-resolution data, they are on average broader and more often completely saturated.

Similarly, we can construct the $W_0^{\lambda 1548}$ distribution for the two velocity ranges. This is shown in Fig. 9. The distributions are normalized such that they represent the differential number of absorbers per \AA per $3 \times 10^5 \text{ km s}^{-1}$ averaged over the velocity range being considered. The distribution for outflow-only systems is therefore obtained simply from the difference of these two distributions and is shown as the solid histogram. It is a much flatter distribution, with a very large excess of strong systems compared to the intervening absorbers. Notably, almost all of the low-velocity narrow absorbers with $W_0^{\lambda 1548} \gtrsim 1.4 \text{\AA}$ can be attributed to outflowing systems. These differences are consistent with the broader FWHM distribution of outflow-systems in Fig. 8.

Table 2. Fraction of quasars containing narrow C IV absorbers.

velocity range (km s^{-1})	all absorbers			outflow-only systems		
	1+	2+	$\langle n \rangle$	1+	2+	$\langle n \rangle$
$1800 < v < 4400$	0.13	0.03	0.17	0.08	0.03	0.11
$0 < v < 3000$	0.21	0.05	0.28	0.08	0.04	0.12
$0 < v < 5000$	0.25	0.08	0.36	0.09	0.05	0.16
$0 < v < 12000$	0.39	0.12	0.60	0.14	0.06	0.25
$v < 3000$	0.27	0.08	0.37			
$v < 5000$	0.31	0.10	0.45			

The values represent the fraction of quasars that exhibit at least one (1+) and at least two (2+) narrow $W_0^{\lambda 1548} \geq 0.3 \text{\AA}$ C IV absorbers in various velocity ranges, as well as the average number of absorbers per spectrum. Values for ‘all’ absorbers are taken directly from the data, while the fractions considering only ‘outflow’ absorbers use our fits to account for environmental and intervening systems, assuming Poissonian statistics.

4.2 How many quasars exhibit outflowing absorbers?

Although $\frac{\partial n}{\partial \beta}$ allows one to calculate the average number of absorbers that will be found in a given range of velocity space per quasar spectrum (i.e., Eqn. 1), it does not contain information on the *fraction of quasars* which exhibit narrow C IV absorption. We show in Table 2 the fraction of spectra that exhibit one or more and two or more narrow C IV absorbers with $W_0^{\lambda 1548} \geq 0.3 \text{\AA}$ for different velocity ranges, as well as the average total number of systems per spectrum, $\langle n \rangle$.

As we are primarily interested in the fraction of quasars exhibiting absorbers that arise in outflows, we use our models for the incidence of environmental and intervening systems as a function of velocity (§3.3.1 and Table 1) to predict the fraction of quasars having a given number of non-outflow absorbers for a given velocity range, assuming Poissonian statistics. While it is likely that intervening absorbers exhibit some degree of clustering, any such possible signal is at levels undetectable in our data (Nestor et al. 2007) and thus the Poissonian assumption is appropriate. The predictions for non-outflow absorbers can then be disentangled from the observed fractions to calculate the fractions for outflowing systems only. These fractions are also shown in Table 2. In this manner we estimate that approximately fourteen per cent of the quasars in our sample exhibit outflows that are detected in narrow C IV absorption over the range $0 < v < 12000 \text{ km s}^{-1}$, where the intrinsic fraction is measured to be non-zero.

It is important to stress that the outflow-only fractions are minima, since we may be counting some outflow-systems as non-outflow ones, and they do not account for systems that we have eliminated due to blending with broad ($\text{FWHM} > 600 \text{ km s}^{-1}$) absorption (§3.1). However, the total fractions (i.e., those including the non-outflow absorbers) represent firm upper limits for the outflow-only fractions. Thus, the overall and calculated outflow-only fractions represent windows in which the true outflow-only fractions lie. For the reasons described in §3.4, we expect that the true outflow-only fractions are near the calculated outflow-only values presented in this table.

5 SUMMARY AND IMPLICATIONS

Our main new results are the following:

1) The distribution of narrow (FWHM < 600 km s⁻¹) C IV absorbers with $W_0^{\lambda 1548} \gtrsim 0.3 \text{ \AA}$ is well described by three components: a Gaussian ‘environmental’ component centred at $v = 0 \text{ km s}^{-1}$ with a deconvolved dispersion of $\approx 450 \text{ km s}^{-1}$, a flat cosmologically-intervening component at $v > 0 \text{ km s}^{-1}$ with $\frac{\partial n}{\partial \beta} \simeq 6.4$, and an outflow component that extends from $v \simeq 750 \text{ km s}^{-1}$ to $v \simeq 12000 \text{ km s}^{-1}$ (Figs. 5 – 7).

2) The outflow-systems account for a large fraction ($\gtrsim 61$ per cent) of all narrow-line absorbers in the velocity range $1800 \text{ km s}^{-1} \lesssim v \lesssim 4400 \text{ km s}^{-1}$. The outflow fraction peaks near $v \simeq 2000 \text{ km s}^{-1}$ at $f_{outflow} \simeq 0.8$. The true outflow fractions might be even higher, and the tail of the distribution might reach beyond $12,000 \text{ km s}^{-1}$, if some of the high-velocity narrow systems ($30000 \text{ km s}^{-1} \lesssim v \lesssim 60000 \text{ km s}^{-1}$) also form in outflows. This possibility is suggested by results from previous studies (e.g., Richards et al. 2001; Misawa et al. 2007).

3) The fraction of quasars with NAL outflows between 0 and $12,000 \text{ km s}^{-1}$ is $\gtrsim 14$ per cent. The fraction of quasars with two or more NAL outflow systems at these velocities is $\gtrsim 6$ per cent.

4) Among the narrow-line systems we consider (FWHM < 600 km s⁻¹), the outflowing absorbers (e.g., at $1800 \text{ km s}^{-1} \lesssim v \lesssim 4400 \text{ km s}^{-1}$) tend to be broader than the intervening ones (at $v \gtrsim 30000 \text{ km s}^{-1}$). The outflow-systems also tend to be stronger and they are more frequently saturated, as measured by $W_0^{\lambda 1548}$ and the C IV doublet ratio.

5) High resolution spectra are needed to examine the flow kinematics, but the measured line widths < 600 km s⁻¹ imply that the projected flow speeds in these NAL outflows are characteristically ~ 10 times larger than the line-of-sight velocity dispersions, i.e., $v/\text{FWHM} \sim 10$.

6) There appears to be a deficit of outflowing NALs at low velocities ($v \lesssim 1500 \text{ km s}^{-1}$ compared to $1500 \text{ km s}^{-1} \lesssim v \lesssim 8000 \text{ km s}^{-1}$).

These results provide important new constraints on models of quasar outflows. For example, the fraction of quasars with NAL outflows ($\gtrsim 14$ per cent) is at least as large as the fraction of quasars with classic (strong and broad) BALs (~ 10 per cent), as measured in similar optically-selected quasar samples (Trump et al. 2006 and refs. therein). Moreover, most of the NAL systems in our study appear in quasars without BALs, and we specifically exclude NALs that are blended with BALs. Therefore, the NAL outflows we measure have no obvious relationship to the BALs. They might represent a wholly different type of outflow phenomenon – one that is perhaps less massive but just as common as the BAL outflows. Perhaps there is an evolutionary relationship where massive BAL outflows tend to dissipate over time to become NAL outflows. Alternatively, the appearance of NAL outflow lines could be simply a different manifestation of a single quasar outflow phenomenon, where our viewing perspective through the flow determines whether we see NALs or BALs (e.g., Elvis et al. 2000, Ganguly et al. 2001). Perhaps the reality in quasars is a mixture of these two scenarios (Hamann & Sabra 2004).

The detection frequencies of the outflow lines provide important constraints on the flow structures. In particular,

the true fraction of quasars with BAL outflows, f_B , is related to the detection frequency by $f_B \gtrsim 0.10$, while the true fraction with NAL outflows is $f_N \gtrsim 0.14$. If there are no orientation biases that affect the detection rates, then the covering factors of the outflows (as seen from the central continuum source) are $\gtrsim 0.14/f_N$ for the NALs and $\sim 0.10/f_B$ for classic BALs. If all quasars have both NAL and BAL outflows as part of a single outflow phenomenon, then the covering factor of outflow gas is $\gtrsim 0.24$. These factors become even larger if we include systems not counted here, e.g., the broader mini-BALs (Rodríguez Hidalgo et al., in prep) and the high-velocity NALs (Misawa et al. 2007, Richards et al. 2001). Moreover, all of these results based on detection frequencies are lower limits if quasars are characteristically fainter when viewed along outflow sightlines (Goodrich et al. 1997, Schmidt & Hines 1999), or if quasars appear obscured and are therefore missed by flux-limited optical surveys when viewed along any range of sightlines. On the other hand, if quasars are preferentially obscured along certain viewing angles by, e.g., a dusty torus, the above covering factors refer only to the unobscured solid-angle.

Further insight into the flow structures comes from the fact that roughly half of the quasars with NAL outflows (6 of the total 14 per cent) have two or more of these outflow features. Thus, the line-of-sight structure is often complex, with either multiple streams or multiple ‘clumps’ contributing to the C IV absorption. In addition, the NAL flow speeds are in the low-to-medium range of BALs, suggesting a similar point of origin for these outflows, but the large ratios of flow speed to line-of-sight velocity dispersion in NALs, $v/\text{FWHM} \sim 10$, contrast markedly with the BALs where typically $v/\text{FWHM} \sim 1$. It is tempting to identify each NAL system with a clump of gas in the flow, but there is no compelling model for these features. Clumps or filaments formed by instabilities at the ragged edge of a BAL flow should be short lived. The measured FWHMs of the NALs, when they are resolved in the SDSS data at several hundred km s⁻¹, suggest highly supersonic expansion.

The possible deficit of low-velocity outflow NALs is another interesting clue, but it also has no straightforward interpretation. This deficit might imply that the inner flow is too ionized for C IV, or that the clumps or streams producing C IV NALs do not form in the inner flow where the speeds are low. There might also be orientation effects that preclude our detection of these clumps or streams of C IV gas near the base of the flow.

Although more work is certainly needed to resolve these questions, NALs represent another important component of quasar outflows. Many studies have focused on the BALs because they are the most obvious and most easily measured of the UV outflow lines. The overall outflow phenomenon is clearly much more diverse, however. Even the NALs and BALs together do not tell the whole story (Hamann & Sabra 2004). These features are at opposite extremes in terms of their FWHMs, but in between is a significant population of ‘mini-BALs’ which have intermediate FWHMs and similar (or perhaps characteristically higher) outflow velocities compared to the NALs and BALs (Rodríguez Hidalgo et al., in prep). The challenge now is to achieve a better physical understanding of this full range of quasar outflow features.

REFERENCES

- Anderson S. F., Weymann R. J., Foltz C. B., Chaffee F. H., Jr., 1987, *AJ*, 94, 278
- Barlow T. A., Sargent W. L. W., 1997, *AJ*, 113, 136
- Becker M. R., et al., 2007, *ApJ*, 669, 905
- Di Matteo T., Springel V., Hernquist L., 2005, *Natur*, 433, 604
- Elvis M., 2000, *ApJ*, 545, 63
- Everett J. E., 2005, *ApJ*, 631, 689
- Foltz C. B., Weymann R. J., Peterson B. M., Sun L., Malkan M. A., Chaffee F. H., Jr., 1986, *ApJ*, 307, 504
- Ganguly R., Bond N. A., Charlton J. C., Eracleous M., Brandt W. N., Churchill C. W., 2001, *ApJ*, 549, 133
- Goodrich R. W., 1997, *ApJ*, 474, 606
- Hall P. B., et al., 2002, *ApJS*, 141, 267
- Hamann F., Korista K. T., Morris S. L., 1993, *ApJ*, 415, 541
- Hamann F., Barlow T. A., Junkkarinen V., Burbidge E. M., 1997a, *ApJ*, 478, 80
- Hamann F., Barlow T. A., Junkkarinen V., 1997b, *ApJ*, 478, 87
- Hamann F., Sabra B., 2004, *ASPC*, 311, 203
- Hamann F., Warner C., Dietrich M., Ferland G., 2007, *ASPC*, 373, 653
- Korista K. T., Voit G. M., Morris S. L., Weymann R. J., 1993, *ApJS*, 88, 357
- McIntosh D. H., Rix H.-W., Rieke M. J., Foltz C. B., 1999, *ApJ*, 517, L73
- Misawa T., Tytler D., Iye M., Storrie-Lombardi L. J., Suzuki N., Wolfe A. M., 2002, *AJ*, 123, 1847
- Misawa T., Charlton J. C., Eracleous M., Ganguly R., Tytler D., Kirkman D., Suzuki N., Lubin D., 2007, *ApJS*, 171, 1
- Moll R., et al., 2007, *A&A*, 463, 513
- Monier E. M., Nestor D. B., Daino M. M., Quider A. M., Rao S. M., Turnshek D. A., 2006, *AAS*, 38, 96
- Mulchaey J. S., 2000, *ARA&A*, 38, 289
- Narayanan D., Hamann F., Barlow T., Burbidge E. M., Cohen R. D., Junkkarinen V., Lyons R., 2004, *ApJ*, 601, 715
- Nestor D. B., Hamann F., Rodriguez Hidalgo P., 2007, *ASPC*, 373, 295
- Nestor D. B., Turnshek D. A., Rao S. M., 2005, *ApJ*, 628, 637
- Outram P. J., Hoyle F., Shanks T., Croom S. M., Boyle B. J., Miller L., Smith R. J., Myers A. D., 2003, *MNRAS*, 342, 483
- Proga D., Stone J. M., Kallman T. R., 2000, *ApJ*, 543, 686
- Proga D., Kallman T. R., 2004, *ApJ*, 616, 688
- Richards G. T., 2001, *ApJS*, 133, 53
- Richards G. T., Vanden Berk D. E., Reichard T. A., Hall P. B., Schneider D. P., SubbaRao M., Thakar A. R., York D. G., 2002, *AJ*, 124, 1
- Ryan-Weber E. V., Pettini M., Madau P., 2006, *MNRAS*, 371, L78
- Sargent W. L. W., Boksenberg A., Steidel C. C., 1988, *ApJS*, 68, 539
- Schmidt, G. D., Hines, D. C., 1999, *ApJ*, 512, 125
- Schneider D. P., et al., 2002, *AJ*, 123, 567
- Scott J., Bechtold J., Dobrzycki A., Kulkarni V. P., 2000, *ApJS*, 130, 67
- Silk J., Rees M. J., 1998, *A&A*, 331, L1
- Songaila A., 2001, *ApJ*, 561, L153
- Stoughton C., et al., 2002, *AJ*, 123, 485
- Trump J. R., et al., 2006, *ApJS*, 165, 1
- Tytler D., Fan X.-M., 1992, *ApJS*, 79, 1
- Vanden Berk D. E., et al., 2001, *AJ*, 122, 549
- Vestergaard M., 2003, *ApJ*, 599, 116
- Weymann R. J., Williams R. E., Peterson B. M., Turnshek D. A., 1979, *ApJ*, 234, 33
- Weymann R. J., Morris S. L., Foltz C. B., Hewett P. C., 1991, *ApJ*, 373, 23
- Wise J. H., Eracleous M., Charlton J. C., Ganguly R., 2004, *ApJ*, 613, 129
- York D. G., et al., 2000, *AJ*, 120, 1579